THE ASTROPHYSICAL JOURNAL, 408:579–585, 1993 May 10

THE MORPHOLOGY AND INTERACTION WITH THE INTERSTELLAR MEDIUM OF THE PLANETARY NEBULA IC 4593

DANIEL B. ZUCKER
Harvard-Smithsonian Center for Astrophysics, 60 Garden Street, Cambridge, MA 02138

AND

NOAM SOKER
Harvard-Smithsonian Center for Astrophysics; and Mathematics-Physics, Oranim—University Division, Tivon 36910, Israel
Received 1992 August 31; accepted 1992 November 2

ABSTRACT

We present a morphological study of the planetary nebula IC 4593, based on our observations in Hα, [O III], and [S II]. From the Hα intensity map, we calculate densities and masses for constituent structures and for the nebula as a whole. We argue that the morphology of IC 4593 suggests that it is moving supersonically through the ISM, and that the ISM shock may be thermally unstable, oscillating between adiabatic and radiative (isothermal) shock conditions. Spectroscopic observations are necessary to further explore the nature of the interaction between IC 4593 and the ISM. An improved understanding of such interactions will greatly expand the potential use of planetary nebulae to probe the ISM.

Subject headings: ISM: structure — planetary nebulae: individual (IC 4593)

1. INTRODUCTION

The idea of studying planetary nebulae which are interacting with the interstellar medium (ISM) to learn more about the ISM itself is discussed in some detail in Borkowski, Sarazin, & Soker (1990). Certain structural features of planetary nebulae (PNs), such as the ratio of a nebula's length along the direction of motion to the length perpendicular to its motion, depend on properties of the nebula and the surrounding ISM, including their respective densities, the age of the nebula, and the nebula's velocity relative to the ISM. The morphology of an interacting nebula also depends on the nature of the interaction—that is, whether adiabatic or radiative conditions predominate in the shock (Soker, Borkowski, & Sarazin 1991). In this paper we present observations of the planetary nebula IC 4593 which suggest that it interacts with the ISM. We analyze the morphology of this nebula and comment on the nature of the interaction, although we leave the quantitative analysis of the surrounding ISM to a future work, which will include both images and spectra of a larger sample of interacting planetary nebulae.

Chu (1989) categorizes IC 4593 as a type I outer shell nebula, with the inner shell expanding supersonically into a faint halo, and Balick (1987) classifies it as an irregular nebula. Cudworth (1974; 1992, private communication) finds the proper motion of this nebula to be ~ 100 km s^{-1} approximately to the west. We chose to study IC 4593 for three reasons: it has a well-defined elliptical shell with two prominent ansae (knotlike projections); it markedly deviates from axial symmetry in the inner region; and its outer morphology suggests motion relative to the ISM (Balick et al. 1992). We first deconvolve the density structure of IC 4593 (§ 3) from its Hα image (§ 2). Because of the deviation from axial symmetry near the center, the interaction with the ISM, and the unknown inclination angle, we cannot use the deconvolution procedure for elliptical PNs of Soker, Zucker, & Balick (1992, hereafter SZB) in this case. Instead we deconvolve the density along different directions from the center, as if the nebula were spherically symmetric (§ 3.1). Although IC 4593 is an elliptical PN, with several asymmetrical features, we obtain reasonable density profiles in some directions. For example, our analysis reveals a "rim," a high-density annulus around and close to the central star (§ 3.2). We then calculate the nebula's total mass and estimate the masses of different constituent structures (§ 3.3).

In § 4 we discuss the dipolar morphology of IC 4593. We find that interaction with the ISM, due to relative motion of IC 4593 and the ISM, is the most likely explanation for such structure. We further argue that some features of the nebula, such as the outlying filaments, suggest that the interaction is unstable, and that the ISM shock oscillates between adiabatic and isothermal (radiative shock) conditions. This is a well-studied shock instability which can occur when the relative velocity is $\gtrsim 140$ km s^{-1} (Gaetz, Edgar, & Chevalier 1988). We present a summary in § 5.

2. OBSERVATIONS

The images of IC 4593 were taken with the Smithsonian Institution's 1.2 m telescope on Mount Hopkins, Arizona, on the nights of 1992 May 24 and 26. The detector used was a 2048 × 2048 pixel Ford CCD, with each pixel projecting $\sim$ 0.″33 on the sky. There were scattered clouds on both nights, and the seeing ranged from 1.″2 to 1.″6. We obtained images in the lines of Hα λ6563, [O III] λ5007, and [S II] λ6717 + λ6731. The Hα filter had a central wavelength of 6566 Å and a bandpass (FWHM) of 22 Å; the [O III] and [S II] filters had central wavelengths of 5008 and 6732 Å, and bandpasses of 20 and 54 Å, respectively. We estimate the contamination of the Hα image by [N II] λ6548 and λ6583 to be less than 10%. All data were reduced using standard IRAF tasks to subtract readout noise, flat-field images, and remove cosmic-ray hits.

To produce the Hα image presented in Figure 1 (Plate 9) we summed two 20 minute exposures and replaced the saturated central region with the corresponding section of a 10 minute exposure, scaled accordingly. To reduce random noise, the image was then smoothed with a 3 × 3 pixel median filter—that is, a sliding window 3 pixels by 3 pixels in size was applied to the image, and the central pixel of the window at each step

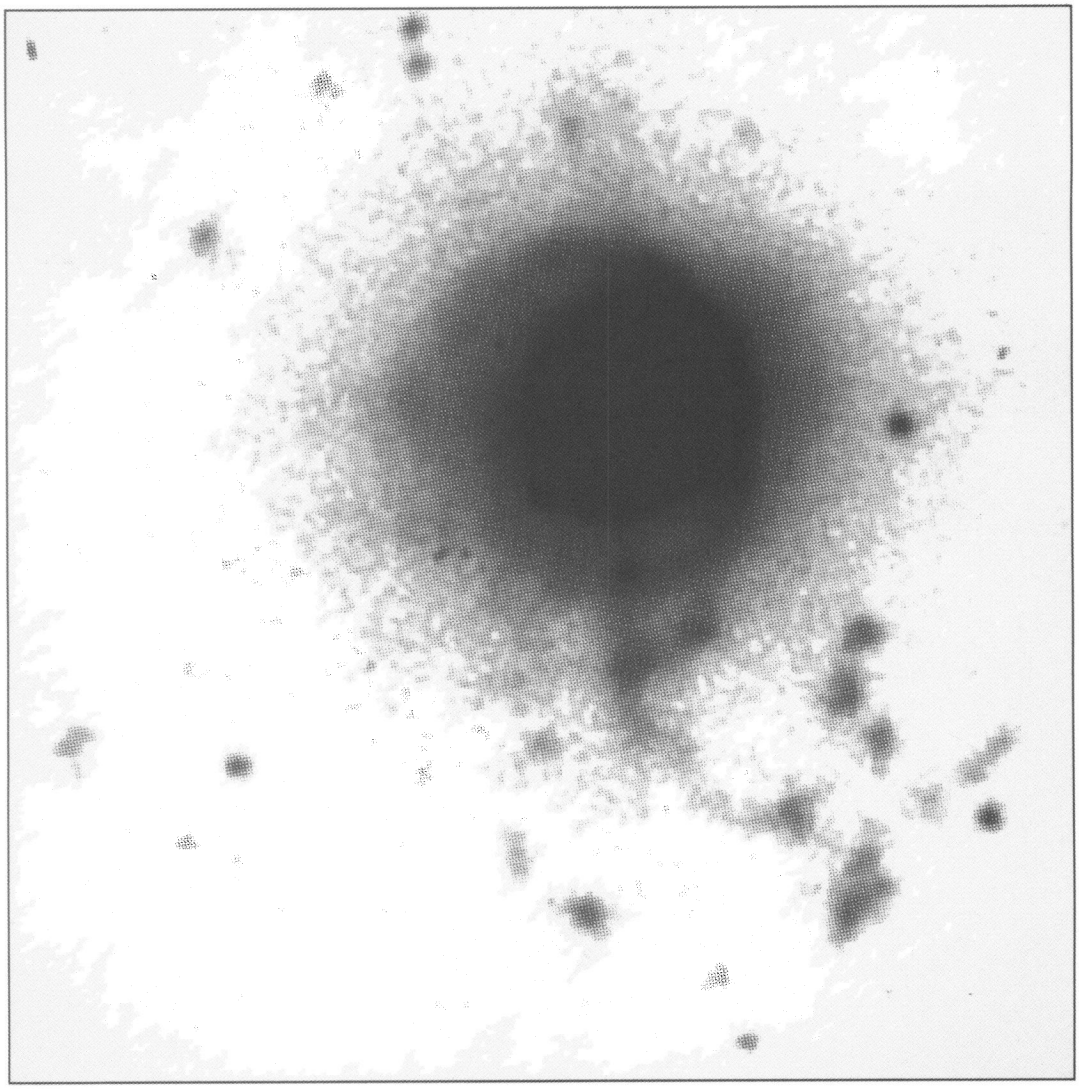

FIG. 1*a*

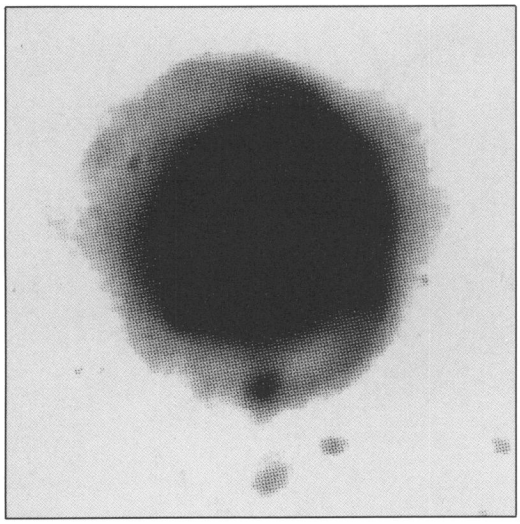

FIG. 1*b*

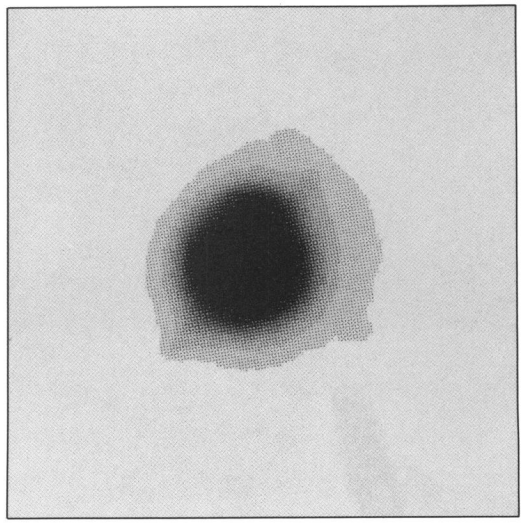

FIG. 1*c*

FIG. 1.—*Top*: Hα image of IC 4593, emphasizing the faint outer regions. The image spans 2′ × 2′. North is up and east is to the left. Darker shades represent bright regions. There are five prominent stars in the field of view, all of them bright, circular sources: two adjacent stars to the northwest, one almost due west near the main body of the nebula, one in the southwest next to the tip of a filament, and one to the southeast of the nebula. *Lower left*: Hα image of IC 4593, emphasizing the main body of the nebula. Scale and orientation are the same as for the top panel. *Lower right*: Hα image of IC 4593, emphasizing the inner regions. Scale and orientation are the same as for the top panel.

was replaced with the median value for all the pixels in the window. The Hα surface brightness contour map shown in Figure 2 was not smoothed. We applied the median smoothing procedure to the [S II] image (a 1 hr exposure) and the [O III] image (a 20 minute integration) before dividing each one by the smoothed Hα image to produce the images in Figure 3.

The outer filaments and condensations of the nebula are shown in the upper panel of Figure 1, which emphasizes the faint regions of the nebula; some are mentioned by Kaler (1974) as a "series of wisps" to the southwest, and several of these outlying structures can be seen in Figure 14 of Balick et al. (1992). (The fuzziness around the bright part of the nebula is low-intensity scattered light and noise.) The lower left panel of Figure 1 shows the main part of the nebula. Around the periphery we see the "bump" (the bulge to the northwest), the "arc" (the bright curve behind the bump), the "arms" (curves on both sides of the arc), and the ansae, knotlike structures which project from the center toward the northwest and the southeast. To the south, note the bright core of condensation A (coincident with the tip of an arm), and condensations B and C below it. (These structures are labeled on the contour map in Figure 2.) The lower right panel of Figure 1 shows the inner regions of IC 4593, including the asymmetric structures surrounding the central star and the "blob," a projection to the north. In Figure 2 all of these constituent structures can be seen clearly; the central star is located at (0, 0), and the major features are marked. We see asymmetry in the central regions in Figure 3*a* (Plate 10), the gray scale image of the [S II]/Hα ratio, although outer structural features are more apparent. The ansae are relatively bright in [S II] (shown by their light color), although the southeast ansa is obscured by noise.

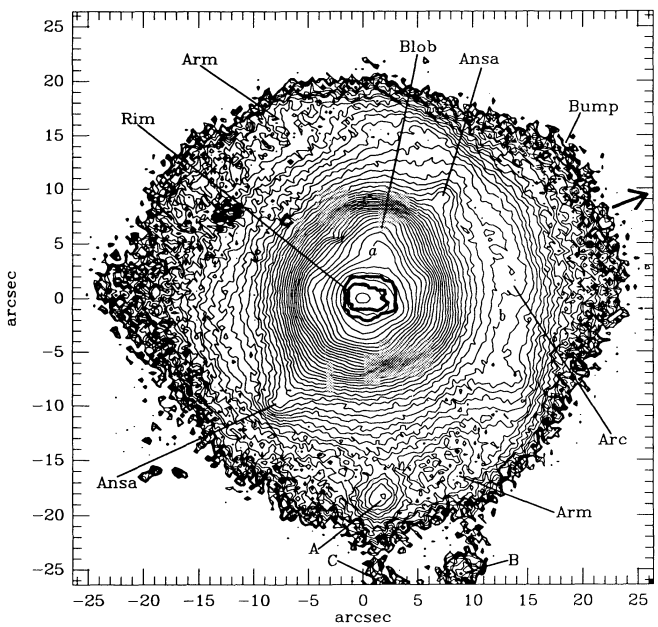

FIG. 2.—Hα surface brightness contour map of IC 4593. The contour levels are in units of $F_{H\alpha}$/arcsec^2, where $F_{H\alpha}$ is the total Hα flux of IC 4593. The levels have a logarithmic spacing of 1.22; the highest contour (just around the center) is 1.8775×10^{-2}, and the lowest is 2×10^{-6}. The level of the peak contour of condensation A is 4.82×10^{-5}, and the levels of contours *a* and *b* are 6.95×10^{-3} and 7.17×10^{-5}, respectively. Features discussed in the paper are labeled. The two thick lines near the center indicate the approximate boundaries of the rim (§ 3.2). The thick arrow points in the presumed direction of the velocity of IC 4593 through the ISM.

Figure 3*b* shows the ratio [O III]/Hα in gray scale. In this image we can see that the bump and the arc are distinct structures. The arc and arms are sharply defined at their outer edges; Balick et al. (1992) comment that these features resemble a bow shock. The ansae and their connections to the central region of the nebula are quite prominent, as are the blob and condensations; their dark color is indicative of relatively weak [O III] emission. These are structures of higher density, as shown in the next section (in Figs. 4 and 5 and in Table 1).

3. THE NEBULA STRUCTURE

3.1. *The Deconvolution Procedure*

Plait & Soker (1990) averaged the Hα flux of the faint round halo of NGC 6826 along concentric annuli before they deconvolved its spherical density profile using the Abel integral equation. SZB assumed an axially symmetric structure for the elliptical planetary nebula NGC 3242 and deconvolved its density structure as a function of the cylindrical coordinates r and z. Because of the blob in the inner region and the bump, arc, and arms in the outer regions, we cannot assume an axially symmetric structure for IC 4593. For the same reason we cannot average the Hα flux along concentric annuli. Instead, following the example of Kupferman (1983), we deconvolve the density along different directions from the center of the nebula, as if the nebula had a spherical structure consistent with the Hα profile along a given direction.

The standard technique for deconvolving density from an intensity map involves solution of the Abel integral equation. Like Wilson & Aller (1951), who deconvolve the density profile of IC 418, we find that using a finite steps procedure, instead of solving the Abel integral equation, is satisfactory for our purposes, and is much simpler to implement. The deconvolution follows the finite steps procedure of SZB, but along a radial direction in spherical geometry. (This is the same as solving for the density versus the radius r in the plane $z = 0$, and for the inclination angle of 90°, in the cylindrical scheme of SZB.) We divide the nebula into concentric spherical shells with constant width dr and assume that the density is constant in each shell. We take the shells' width to be $dr = 0''.066$, although we found that acceptable results are obtained even for widths as large as $dr = 0''.66$. Moving from the edge toward the center, we find the volume emissivity in each shell ϵ_i(ergs s^{-1} cm^{-3}). The density is obtained from the expression for the volume emissivity

$$\epsilon = \Lambda n_e n_p = 7.28 \times 10^{-22} \left(\frac{\rho}{10^{-22}\ \mathrm{g\ cm^{-3}}} \right)^2 \mathrm{ergs\ s^{-1}\ cm^{-3}}\ , \tag{3.1}$$

where for an electron temperature of $T_e = 10^4$ K and electron density of $\sim$few $\times 10^3$ cm^{-3} the Hα emission coefficient is $\Lambda = 3.54 \times 10^{-25}$ ergs s^{-1} cm^{-3} (Pottasch 1984), n_p and n_e are the proton and electron densities, respectively, and we have assumed fully ionized solar composition gas in the second equality.

Since the volume of each shell scales as d^3, where d is the distance from Earth to the nebula, and since the flux, measured on Earth (and corrected for extinction), goes as $F_{H\alpha} \propto d^{-2}$, the emissivity varies as $\epsilon \propto F_{H\alpha}/d$. Taking into account the great uncertainty in the distance to IC 4593 (Phillips & Pottasch 1984 obtain $d = 3.76$ kpc, while Heap & Augensen 1987 use $d = 2.1$ kpc), we adopt a distance of $d = 2.5$ kpc. Based on the

1993ApJ...408..579Z

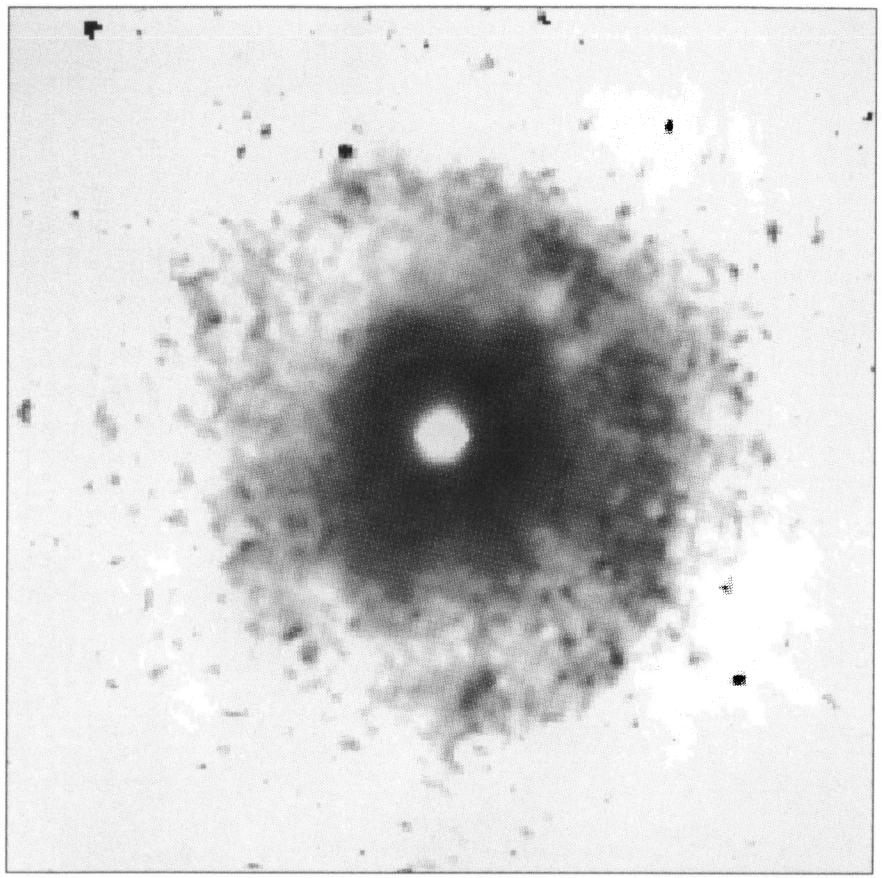

FIG. 3*a*

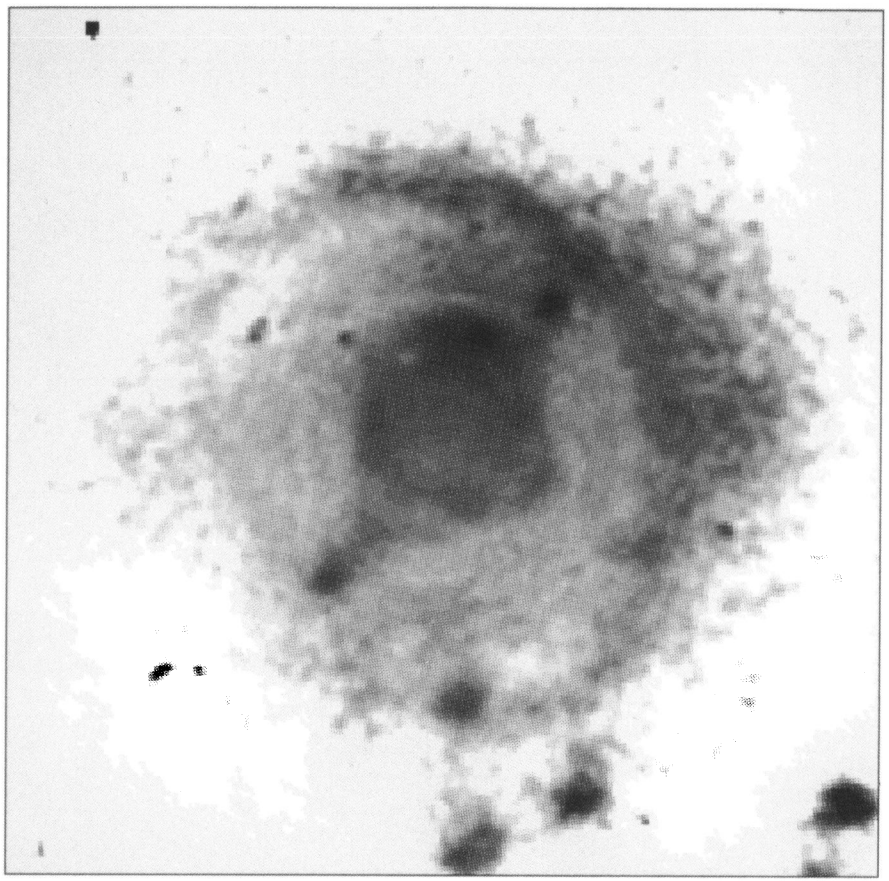

FIG. 3*b*

FIG. 3.—(*a*) Gray-scale image of IC 4593 showing the ratio [S II]/Hα. Features with smaller ratios appear darker. The two ansae are relatively bright, although the southeast ansa is almost obscured by noise. The two bright radial lines at ~320° and ~230° are probably diffraction spokes from the central star in the [S II] image. The image measures 1′ × 1′. North is up and east is to the left. (*b*) Gray-scale image of IC 4593 showing the ratio [O III]/Hα. The ansae and blob are dark (indicating a low ratio), as are the arc and condensations. The scale and orientation are the same as for (*a*).

Hβ flux of IC 4593 (Acker et al. 1991), we assume a total Hα flux corrected for extinction of $F_{H\alpha} = 1.3 \times 10^{-10}$ ergs s^{-1} cm^{-2}. As did Preite-Martinez et al. (1989), we take the electron temperature to be $T_e = 10^4$ K, and we include the crude dependence of Λ on the electron temperature near 10^4 K: $\Lambda \propto T_e^{-0.94}$. The density at any point in the nebula, ρ, is scaled with the density we calculate here, ρ_{here}, according to

$$\frac{\rho}{\rho_{here}} = \left(\frac{d}{2.5\ \mathrm{kpc}}\right)^{-1/2} \times \left(\frac{F_{H\alpha}}{1.3 \times 10^{-10}\ \mathrm{ergs\ s^{-1}\ cm^{-3}}}\right)^{1/2} \left(\frac{T_e}{10^4\ \mathrm{K}}\right)^{0.47}. \quad (3.2)$$

The mass is obtained by integrating the density over the volume of the nebula. Since the volume of any part of the nebula is proportional to d^3, the masses of the different parts of the nebula are scaled with the masses given in this paper M_{here} as

$$\frac{M}{M_{here}} = \left(\frac{d}{2.5\ \mathrm{kpc}}\right)^{5/2} \times \left(\frac{F_{H\alpha}}{1.3 \times 10^{-10}\ \mathrm{ergs\ s^{-1}\ cm^{-3}}}\right)^{1/2} \left(\frac{T_e}{10^4\ \mathrm{K}}\right)^{0.47}. \quad (3.3)$$

We derive approximate masses of the blob, ansae, and condensations by assuming spherical symmetry with constant density for each of these constituents. The emission measure in units of energy—the integrated emissivity along the line of sight—through the center of a sphere with constant density is EMe(ergs s^{-1} cm^{-2}) = 2aε, where a is the radius of the sphere. From the emission measure EMe we obtain the emissivity, the density as in equation (3.1), and the mass $M = \rho 4\pi a^3/3$. The emission measure (in units of energy) at a given pixel is found from the total flux of this pixel I(ergs s^{-1} cm^{-2}) with the formula EMe $= 4\pi d^2 I/A$, where A(cm^2) is the area on the nebula covered by the given CCD pixel. To find the emission measure of any constituent structure, we use the excess surface brightness at its center relative to the surface brightness in its immediate surroundings.

3.2. *The Density Profile*

The intensity profiles along six directions are given in the upper panels of Figure 4. (In this paper, angular coordinates are counterclockwise from due north, with the central star at the origin.) The density profiles along these directions, which were deconvolved assuming that the nebula has a spherical structure determined by the intensity profile along each given direction, are given in the lower panels of Figure 4. These directions were chosen so as not to contain the ansae and the blob, so that the assumption of sphericity is reasonable; this assumption, however, cannot be made for the bump, in the direction 280°. Some features that are defined in Figure 2 are marked on the graphs.

The density profile reveals the "rim," a feature that is impossible to recognize from the intensity map itself. The rim is a high-density shell which is formed by the pressure of the fast wind on the inner boundary of the superwind, and it is seen as a bright thin annulus in the innermost region of many PNs

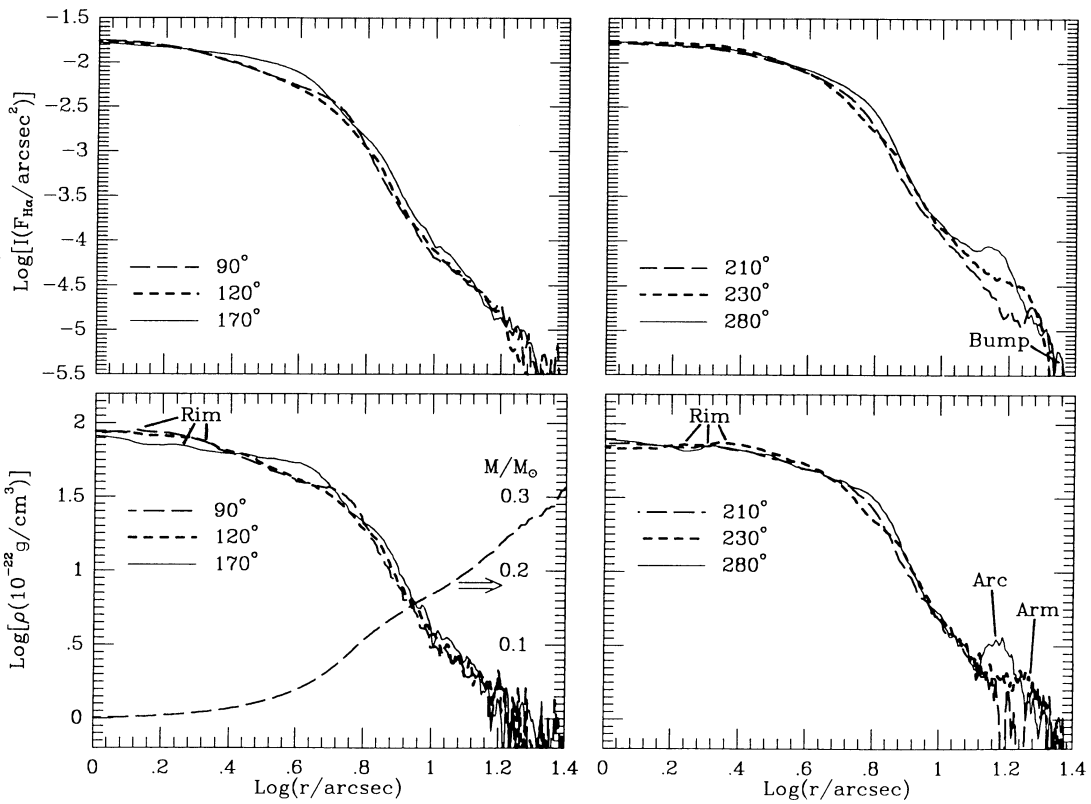

FIG. 4.—*Upper panels*: Hα intensity vs. radius along six different directions from the central star of IC 4593. Angles are measured counterclockwise from north, and $F_{H\alpha}$ is the total flux from IC 4593. *Lower panels*: The density profiles along these directions, deconvolved assuming that the nebula has a spherical structure determined by the intensity profile along each given direction. For the direction 90° the total mass enclosed in a sphere vs. the radius of the sphere is also presented.

(Frank, Balick, & Riley 1990). The central star of IC 4593 generates a fast wind with a velocity of $v = 1400$ km s^{-1} and a mass-loss rate of $\dot{M} \simeq 4.2 \times 10^{-8}\ M_\odot$ yr^{-1} (Cerruti-Sola & Perinotto 1989). This is relatively slow and intense for a fast wind, suggesting that the fast wind is young. Consequently in this nebula we would expect to see a concentric ring close to the central star, as there would not have been time for the interface between the fast wind and the superwind to have traveled very far. We find that there are two local maxima in the density profile near $r = 2''$, which are plotted on top of the Hα intensity contour map (thick lines in Fig. 2). Because of the noise introduced in the deconvolution process and the low resolution of the initial image (relative to the distance of the postulated rim from the center), we cannot be sure that the structure seen in the density profile is in fact a rim. However, considering the properties of the fast wind, we assume that it is a rim, bounded by the two local maxima. The density in the region between the rim and the central star is very low, but due to contamination from the central star and limited seeing conditions the density given in Figure 4 is an overestimate.

The mass enclosed in a sphere versus radius is presented in Figure 4 for the density profile along the eastern direction (90°). Different directions gives different total masses, in the range of 0.3–0.45 $M_\odot$, with higher masses in the north and west. We can estimate the excess mass in the northwest direction if we assume that this bright region—which includes the bump, arc, and part of the arms—has the structure of a cap. Then, since we go from the edge inward in the density deconvolution, the density profile of this region is not influenced by the fact that the outer cap region is not a full sphere. (Note that the calculated densities in regions inside the cap to the northwest are not reliable.) We assume that the outer cap region stretches from 210° to 10°, with its symmetry axis in the direction of 290°, and that it extends from 12″ to 22″. We find the excess mass in this cap region to be $\sim 0.04\ M_\odot$. The total mass of the nebula inside a radius of 25″ is therefore $M_{\rm nebula} = 0.37 \pm 0.03\ M_\odot$, scaled with the parameters given in equation (3.3).

We note that within a radius of 6″ the mass is 0.1 $M_\odot$. With an assumed distance of $d = 3.76$ kpc and a nebula radius of 6″, Phillips & Pottasch (1984) find the total mass of IC 4593 to be 0.3 $M_\odot$. Scaling their mass to a distance of $d = 2.5$ kpc gives a mass of 0.09 $M_\odot$ inside 6″. This is quite close to our value, given the many uncertainties.

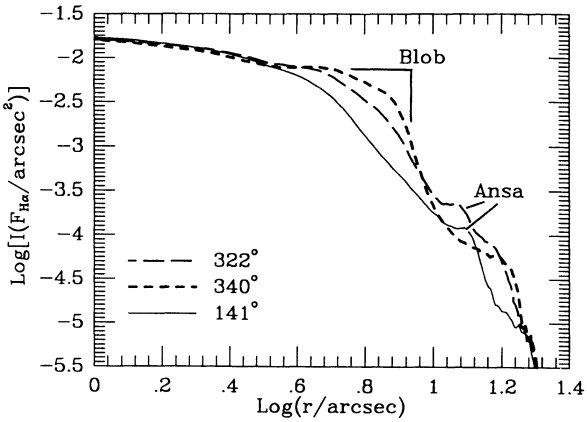

FIG. 5.—As in the upper panels of Fig. 4, but along different directions.

3.3. *The Blob, Ansae, and Condensations*

The intensity profiles along the directions which pass through the centers of the ansae and blob are given in Figure 5. We calculate the masses of the blob, ansae, and condensations by assuming a spherical structure of constant density, as explained in § 3.1. The radius, location, electron density, and mass of each of these constituents are given in Table 1. Because of these strong assumptions, the above masses should be considered as very crude estimates. The masses are scaled with distance, Hα flux, and electron temperature according to equation (3.3).

In general, ansae are thought to be the leading heads of jets (one jet on each side) moving faster than the rest of the nebula (Balick, Preston, & Icke 1987). Soker (1992) proposes a model in which there are two classes of jets and ansae, with a continuous transition between them. During the evolution of a post-AGB star, the stellar radius decreases as the envelope mass

TABLE 1

MASSES OF DIFFERENT CONSTITUENTS OF IC 4593

Constituent	Radius	Center (r, ϕ)	n_e (cm^{-3})	Mass ($M_\odot$)
Main nebula	~24″	(0″, 0°)	Fig. 4	0.37 ± 0.03
blob	2.5	(6, 345)	~2300	$\sim 8 \times 10^{-3}$
Northern ansa	1.2	(11.8, 322)	~440	$\sim 1.7 \times 10^{-4}$
Southern ansa	1.2	(12.4, 141)	~370	$\sim 1.4 \times 10^{-4}$
Cap	...	(17, 290)	Fig. 4 (280°)	~0.04
Condensation A	~2.8	(18.4, 185)	~200	$\sim 1 \times 10^{-3}$
Condensation B	~1.9	(26.8, 200)	~150	$\sim 2 \times 10^{-4}$
Condensation C	~2.3	(29.0, 185)	~125	$\sim 3 \times 10^{-4}$
Condensation D	~1.3	(32.0, 8.5)	~100	$\sim 5 \times 10^{-5}$
Condensation E	~2.6	(38.0, 228)	~140	$\sim 5 \times 10^{-4}$
Condensation F	~2.7	(41.5, 219)	~115	$\sim 5 \times 10^{-4}$
Condensation G	~2.4	(48, 219)	~125	$\sim 4 \times 10^{-4}$
Condensation H	~2.1	(50, 67.5)	~125	$\sim 2.5 \times 10^{-4}$
Condensation I	~2.5	(50, 204)	~95	$\sim 3 \times 10^{-4}$
Condensation J	~2.7	(57, 176.5)	~125	$\sim 5 \times 10^{-4}$
Condensation K	~1.8	(57.5, 209)	~120	$\sim 1.5 \times 10^{-4}$
Condensation L	~1.8	(61.5, 209)	~130	$\sim 2 \times 10^{-4}$
Condensation M	~2.3	(62.5, 205)	~140	$\sim 4 \times 10^{-4}$
Condensation N	~2.7	(72, 121.5)	~90	$\sim 4 \times 10^{-4}$

does. The contraction with decreasing envelope mass becomes more and more rapid, with a sharp drop in radius at an envelope mass of $\sim 6 \times 10^{-4}\ M_\odot$. The trend reverses (i.e., the decrease in radius slows) at $R \simeq 30\ R_\odot$. These two phases of contraction can give rise to the two types of jets proposed by Soker (1992). The first type of jet—slow jets—is formed at the very end of the AGB and at the beginning of the post-AGB phase. Their velocities are $\gtrsim 50$ km s^{-1}, and their total masses are $\lesssim 10^{-3}\ M_\odot$. The second class—fast jets—is formed during the post AGB phase and at the beginning of the PN phase. Their velocities are ~ 100–300 km s^{-1}, and their total masses are $\lesssim 10^{-4}\ M_\odot$. If the total mass of $3 \times 10^{-4}\ M_\odot$ of the two ansae in Table 1 is correct, then the ansae of IC 4593 belong to the slow-jets classification of the above model. However, we could have easily overestimated their masses by a factor of ~ 5. The velocity of the jets is another indicator as to their nature. If the [N II] velocity in the measurements of Anandarao & Banerjee (1988) corresponds to the ansae, then their line-of-sight velocities are $v_l = 47$ km s^{-1} for the northern ansa, and $v_l = -41$ km s^{-1} for the southern ansa. Since the data of Anandarao & Banerjee (1988) lack spatial resolution, it is hard to tell if these velocities actually correspond to the ansae. Let us assume that the ansae have a line-of-sight velocity of $v_l \simeq 45$ km s^{-1}. If indeed the ansa velocities are less than 100 km s^{-1}, then the inclination angle θ (the angle of the line connecting the two ansae to the line of sight) must be smaller than $\sim 60°$. Further assuming that the ansa velocities were constant during their evolution, the age of the ansae is

$$\tau_{\rm ansa} = 1800\ {\rm yr} \left(\frac{\tan\theta}{\tan 60°}\right)^{-1} \times \left(\frac{d}{2.5\ {\rm kpc}}\right)\left(\frac{r_{\rm ansa}}{12''}\right)\left(\frac{v_l}{45\ {\rm km\ s^{-1}}}\right)^{-1}, \quad (3.4)$$

where $r_{\rm ansa}$ is the projected distance of an ansa from the central star.

We are not aware of any model or explanation for the existence of the blob. Judging from its location and mass, it is likely that it was formed at very late stages of the AGB, or even during the post-AGB phase. The blob is prominent in [N II] (Balick 1987) and faint in [O III] (Fig. 3*b*), as are the ansae; this further suggests that the density in the blob is higher than in its surroundings. The center of the blob has a projected angle of 23° from the northern ansa. It is possible, however, that the true angle is 90°, and that the blob lies in the plane perpendicular to the line joining the ansae.

4. INTERACTION WITH THE ISM

A prominent morphological feature of interacting nebulae is that the nebular edge in the direction of motion is the closest to the central star (e.g., the PN A35 [Jacoby 1981] and the nebula around the cataclysmic variable 0623+71 [Hollis et al. 1992]). Although we cannot see it in Figures 1 and 2, Figure 3 shows that the bump and the arc are separate structures. Since the bump seems to have a different origin (see below), we consider the arc to be the edge of the nebula and consequently believe that this condition applies to IC 4593. The [S II]/Hα and [O III]/Hα images present what appears to be a bow shock; this morphology, seen in the Hα + [N II] image of Balick et al. (1992), led these authors to suggest that it results from interaction with the ISM. We must be cautious about this interpretation, however, since Figure 3 also shows that the overall morphology of IC 4593 is quite complicated.

One alternate hypothesis is that the arc and arms (see Fig. 2) are simply part of an elliptical shell. We believe that this is unlikely, since it cannot account for the fact that the northwest side (the location of the postulated bow shock) is much brighter, and that the line connecting the two ansae is not aligned with any hypothetical shell axis. A second possibility is that the asymmetry of the outer regions of the nebula is somehow linked to the asymmetrical features of the inner region $r \lesssim 10''$, such as the blob to the north. In particular, the [S II]/Hα image (Fig. 3*a*) shows an inner arc $r \simeq 5''$, in the same direction (west) as the outer arc at $r \simeq 15''$. The asymmetry in the outer region, however, is much more pronounced than in the inner region, and in Figure 3*b* ([O III]/Hα) is oriented more to the north, which would support the model for interaction with the ISM.

As we discussed above, the morphology of the outer regions of IC 4593 strongly suggests that the nebula is moving relative to the ISM toward the northwest, in the direction $\sim 290°$ (thick arrow in Fig. 2). However, we would further argue that specific morphological features gives us an indication as to the nature of the interaction between the nebula and the ISM. To illustrate this, we present some results of numerical simulations by Soker et al. (1991).

Soker et al. (1991) simulate the supersonic motion of PNs through the ISM with a two-dimensional hydrodynamical scheme. They present two limiting types of interactions: adiabatic and isothermal. In the adiabatic case the postshock ISM does not have time to cool as it flows around the nebula, while in the isothermal case the ISM cooling time is much shorter than the flow time. In Figure 6 we show the density contour maps of two of their models, one adiabatic (their Fig. 3, of model C) and one isothermal (their model H). In these maps (X, Y) are cylindrical coordinates, with Y the symmetry axis and X the distance from the symmetry axis. The nebula is moving in the positive Y direction (upward in Fig. 6), and the central star is located at (0, 0). The two models have completely different physical parameters, but for the purpose of our qualitative discussion the time and levels of the density contours in Figure 6 are not important. In the adiabatic case the ISM shock location can be clearly seen (marked by contour levels 0.006 and 0.01), while in the isothermal case this shock coincides with the outer boundary of the PN shell. Again we stress that because Soker et al. (1991) choose specific physical parameters for their simulations and since many physical parameters relevant to IC 4593 (e.g., the density of the surrounding ISM and the relative velocity) are unknown, only a qualitative comparison is reasonable. They, for example, assume a constant-velocity, expanding thin PN shell; this is not the case for IC 4593, where it is the continuous AGB wind that is interacting with the ISM, not the dense shell of the nebula (corresponding to the superwind), which is located closer to the central star.

From morphological considerations, we find that the bump of IC 4593 (Fig. 2) can be explained as the "bump" formed by a Rayleigh-Taylor instability in the leading front of a nebula in the adiabatic case. The Rayleigh-Taylor instability in Figure 6 appears as a low-density hollow region along the axis, and a high-density torus (in three dimensions) around it. Similarly the arms of IC 4593 can be interpreted morphologically as the "arms" in the isothermal case. Both of these features are marked in Figure 6. Note that Figures 1 and 2 are intensity maps which give the integrated flux along each line of sight,

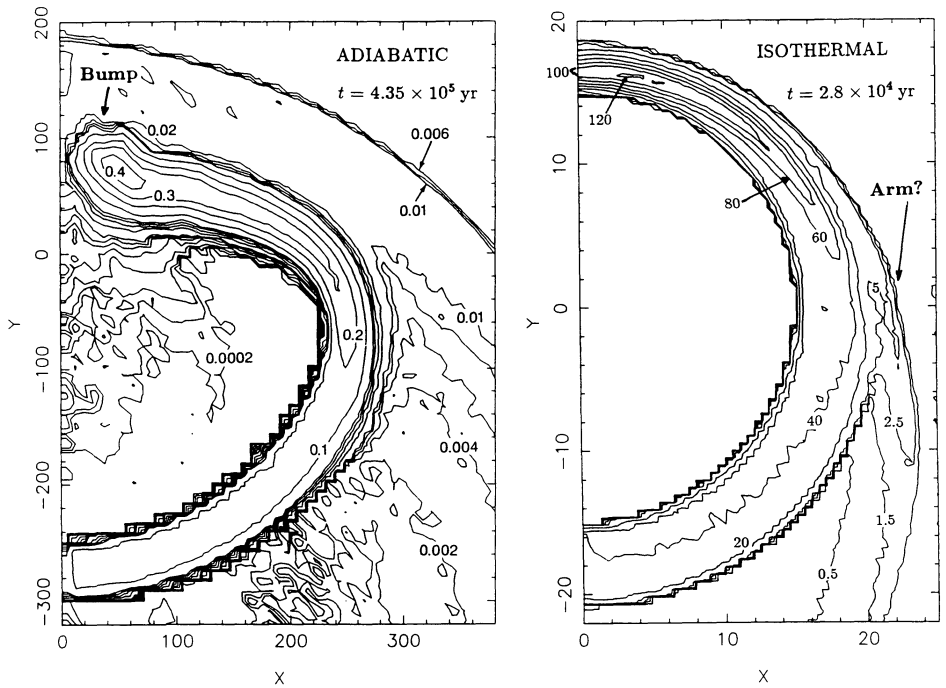

FIG. 6.—Density contour map for an adiabatic simulation (*left*) and an isothermal simulation (*right*) from Soker et al. (1991). The units on the axes are 10^{17} cm, and density levels are in units of 10^{-24} g cm^{-3}.

while the models shown in Figure 6 present density levels in the symmetry plane. This distinction limits us to a purely morphological comparison of these structures.

The condensations and filaments seen in the outer regions of the nebula could be the result of thermal instabilities in the shocked ISM, or in extended nebular material. The existence of features resembling both the isothermal and the adiabatic cases (i.e., the arms and bump), and what appear to be condensations and filaments of thermal instability, suggests that the interaction process oscillates between adiabatic and isothermal conditions. The overstability of radiative shocks, in which the shock location oscillates with time, is a well-studied phenomenon. Gaetz et al. (1988) examined this process in great detail for one-dimensional flows, and Gouveia Dal Pino & Benz (1993) found such instabilities in their three-dimensional simulations of jet propagation through the ISM. Gaetz et al. calculate that a shock becomes unstable at a relative velocity $v_{\rm rel} \gtrsim 140$ km s^{-1}, and they speculate that the instability can also occur for $v_{\rm rel} \lesssim 90$ km s^{-1}. A velocity of ~ 140 km s^{-1} through the ISM can be typical for objects at 1.6 kpc above the Galactic disk—the height of IC 4593, given our assumed distance of 2.5 kpc. Indeed, Cudworth (1974; 1992, private communication) finds that the absolute proper motion of this nebula is ~ 100 km s^{-1} approximately to the west, which may be sufficient for such instabilities to occur.

With PNs as distant as several kpc revealing their interaction with the ISM, we can expect to collect data—both images and spectra—on a large sample of interacting PNs in future observations. In light of the fact that other PNs which interact with the ISM also have filaments around them (e.g., A35; Jacoby 1981), it is possible that shock overstability is a common phenomenon. A careful theoretical study—involving numerical simulations—of time-dependent interaction, taking into account a realistic cooling function, is crucial for understanding such interactions.

5. SUMMARY

We observed the planetary nebula IC 4593, obtaining images in Hα (Fig. 1), [S II] (Fig. 3*a*), and [O III] (Fig. 3*b*). We used these images to analyze the morphology of the nebula, and deconvolved the densities and masses of the entire nebula and of the constituent structures (Table 1) from the Hα intensity map (Fig. 2). The calculated density profile reveals a dense ring—the rim—at $\sim 2''$ from the center (Fig. 4), which is not visible in images of the intensity; this illustrates the importance of deconvolving density profiles for nebulae in order to understand their structure and evolution.

The morphology of the outer regions (Figs. 1 and 3) suggests that IC 4593 is moving relative to the ISM (in the direction indicated on Fig. 2) and is interacting with the ISM in a complex manner. Based on features such as the outlying filaments and condensations (upper panel of Fig. 1), we suggest that the ISM shock may be thermally unstable and oscillates between adiabatic and isothermal conditions. A further exploration of the nature of the interaction between IC 4593 (and other interacting nebulae) and the ISM, including both observations and theoretical work, will serve as an essential step toward using planetary nebulae to study the ISM.

We thank Susan Durham for the use of her filters, and thank John Raymond for some very helpful discussions. We also thank Barbara Whitney, Kazimierz Borkowski, and You-Hua Chu for their careful readings of this paper. This work has been supported by NASA grant NAG 5-1388.

REFERENCES

Acker, A., Stenholm, B., Tylenda, R., & Raytchev, B. 1991, A&AS, 90, 89
Anandarao, B. G., & Banerjee, D. P. K. 1988, A&A, 202, 215
Balick, B. 1987, AJ, 94, 671
Balick, B., Gonzalez, G., Frank, A., & Jaboby, G. 1992, ApJ, 392, 582
Balick, B., Preston, H. L., & Icke, V. 1987, AJ, 94, 1641
Borkowski, K. J., Sarazin, C. L., & Soker, N. 1990, ApJ, 360, 173
Cerruti-Sola, M., & Perinotto, M. 1989, ApJ, 345, 339
Chu, Y.-H. 1989, in IAU Symp. 131, Planetary Nebulae, ed. Silvia Torres-Peimbert (Dordrecht: Kluwer), 105
Cudworth, K. M. 1974, AJ, 79, 1384
Frank, A., Balick, B., & Riley, J. 1990, AJ, 100, 1903
Gaetz, T. J., Edgar, R. J., & Chevalier, R. A. 1988, ApJ, 329, 927
Gouveia Dal Pino, E. M., & Benz, W. 1993, ApJ, submitted
Heap, S. R., & Augensen, H. J. 1987, ApJ, 313, 268
Hollis, J. M., Oliversen, R. J., Wagner, R. M., & Feibelman, W. A. 1992, ApJ, 393, 217
Jacoby, G. H. 1981, ApJ, 244, 903
Kaler, J. B. 1974, AJ, 79, 594
Kupferman, P. N. 1983, ApJ, 266, 689
Phillips, J. P., & Pottasch, S. R. 1984, A&A, 130, 91
Plait, P., & Soker, N. 1990, AJ, 99, 1883
Pottasch, S. R. 1984, Planetary Nebulae (Dordrecht: Reidel)
Preite-Martinez, A., Acker, A., Koppen, J., & Stenholm, B. 1989, A&AS, 81, 309
Soker, N. 1992, ApJ, 389, 628
Soker, N., Borkowski, K. J., & Sarazin, C. L. 1991, AJ, 102, 1381
Soker, N., Zucker, D. B., & Balick, B. 1992, AJ, 104, 2151
Wilson, O. C., & Aller, L. H. 1951, ApJ, 114, 421